Marco A. Marra[1]
Orthopaedic Research Laboratory,
Radboud Institute for Health Sciences,
Radboud University Medical Center,
P.O. Box 9101,
HB Nijmegen 6500,
The Netherlands
e-mail: Marco.Marra@radboudumc.nl

Valentine Vanheule
N. V. Materialise,
Technologielaan 15,
Leuven 3001, Belgium
e-mail: Valentine.Vanheule@kuleuven.be

René Fluit
Faculty of Engineering Technology,
Laboratory of Biomechanical Engineering,
University of Twente,
P.B. 217, Gebouw Horstring,
Enschede 7500 AE, The Netherlands
e-mail: R.Fluit@utwente.nl

Bart H. F. J. M. Koopman
Faculty of Engineering Technology,
Laboratory of Biomechanical Engineering,
University of Twente,
P.B. 217, Gebouw Horstring,
Enschede 7500 AE, The Netherlands
e-mail: H.F.J.M.Koopman@ctw.utwente.nl

John Rasmussen
Department of Mechanical
and Manufacturing Engineering,
Aalborg University,
Fibigerstrade 16,
Aalborg East DK-9220, Denmark
e-mail: jr@m-tech.aau.dk

Nico Verdonschot
Orthopaedic Research Laboratory,
Radboud Institute for Health Sciences,
Radboud University Medical Center,
P.O. Box 9101,
HB Nijmegen 6500, The Netherlands
e-mail: Nico.Verdonschot@radboudumc.nl

Michael S. Andersen
Department of Mechanical
and Manufacturing Engineering,
Aalborg University,
Fibigerstraede 16,
Aalborg East DK-9220, Denmark
e-mail: msa@m-tech.aau.dk

A Subject-Specific Musculoskeletal Modeling Framework to Predict In Vivo Mechanics of Total Knee Arthroplasty

Musculoskeletal (MS) models should be able to integrate patient-specific MS architecture and undergo thorough validation prior to their introduction into clinical practice. We present a methodology to develop subject-specific models able to simultaneously predict muscle, ligament, and knee joint contact forces along with secondary knee kinematics. The MS architecture of a generic cadaver-based model was scaled using an advanced morphing technique to the subject-specific morphology of a patient implanted with an instrumented total knee arthroplasty (TKA) available in the fifth "grand challenge competition to predict in vivo knee loads" dataset. We implemented two separate knee models, one employing traditional hinge constraints, which was solved using an inverse dynamics technique, and another one using an 11-degree-of-freedom (DOF) representation of the tibiofemoral (TF) and patellofemoral (PF) joints, which was solved using a combined inverse dynamic and quasi-static analysis, called force-dependent kinematics (FDK). TF joint forces for one gait and one right-turn trial and secondary knee kinematics for one unloaded leg-swing trial were predicted and evaluated using experimental data available in the grand challenge dataset. Total compressive TF contact forces were predicted by both hinge and FDK knee models with a root-mean-square error (RMSE) and a coefficient of determination (R^2) smaller than 0.3 body weight (BW) and equal to 0.9 in the gait trial simulation and smaller than 0.4 BW and larger than 0.8 in the right-turn trial simulation, respectively. Total, medial, and lateral TF joint contact force predictions were highly similar, regardless of the type of knee model used. Medial (respectively lateral) TF forces were over- (respectively, under-) predicted with a magnitude error of $M < 0.2$ (respectively > -0.4) in the gait trial, and under- (respectively, over-) predicted with a magnitude error of $M > -0.4$ (respectively < 0.3) in the right-turn trial. Secondary knee kinematics from the unloaded leg-swing trial were overall better approximated using the FDK model (average Sprague and Geers' combined error $C = 0.06$) than when using a hinged knee model ($C = 0.34$). The proposed modeling approach allows detailed subject-specific scaling and personalization and does not contain any nonphysiological parameters. This modeling framework has potential applications in aiding the clinical decision-making in orthopedics procedures and as a tool for virtual implant design. [DOI: 10.1115/1.4029258]

Introduction

Movements and loads of MS systems are governed by complex interactions between the forces of muscles, ligaments, bones, and a variety of other soft tissues, and the surrounding environment. Muscle, ligament, and joint contact forces acting within the body are, however, very difficult to measure in vivo, since invasive procedures would be required. A number of studies on patients with instrumented prostheses have recently made available internal joint load measurements in vivo [1–4]. In a few cases, such procedures led to the release of extensive databases containing joint forces recorded in vivo in patients who received a telemetric prosthesis [5,6]. Remarkable examples of such procedures are the OrthoLoad project [7], providing hip, shoulder, knee, vertebral body, and spine fixator forces of implanted patients, and the "grand challenge competition to predict in vivo knee loads" [8],

[1]Corresponding author.

Manuscript received October 2, 2014; final manuscript received November 25, 2014; published online January 26, 2015. Editor: Beth A. Winkelstein.

based on the most comprehensive dataset currently available for subjects implanted with a telemetric TKA. The experimental material provided by these initiatives has stimulated the MS modeling community to improve the clinical utility of their computational models through extensive validation. Unfortunately, such valuable data are only available for a limited number of selected patients and provide insight into the functioning of a particular type of prosthesis under specific conditions.

Although these datasets provide highly valuable information, they do not include any information on forces generated by the muscles or transmitted through the ligaments. Knowledge of muscle, ligament, and joint contact forces would be highly beneficial from a clinical perspective, but their direct measurement is not feasible in a clinical setting and patients with an instrumented prosthesis are rare. Predictive capabilities of computational MS models are, therefore, being considered to gain dynamic and objective information on the condition of individual patients [9]. This, in turn, would aid the formulation of quantitative and patient-specific indications for an optimal treatment [10–15]. Such an approach can potentially overcome the limitations of current practice, in which treatments are based on subjective, static, and mostly qualitative assessment [8]. Although MS models have been extensively used in many fields including ergonomics [16,17], occupational health [18], gait analysis and training [19], and evaluation of prosthetic design [20–22], the lack of proper validation has delayed the introduction of MS models into clinical practice [23]. Muscle, ligament, and joint forces are generally the outputs of an MS model and a common practice is to evaluate model-predicted muscle activities using surface electromyographic (EMG) signals recorded from the main muscles, as an indirect validation of muscle forces [9]. However, this approach proves unsuccessful for validating dynamic tasks, in which the relationship between individual muscle forces and their EMG signals is complex [24,25]. On the other hand, muscle forces are the main determinants of internal joint forces [26], so if the latter are being predicted correctly, it is likely that muscle force predictions are also reasonably accurate.

A few works appeared in the recent literature that dealt with prediction of knee joint mechanics and evaluation of MS model predictions using experimental data. Thelen et al. [27] developed a modeling framework for the concurrent simulation of body-level dynamics and joint mechanics during gait. Their method was based on forward-dynamics coupled with computed muscle control and could predict muscle activations and TF forces in an elastic foundation model of TKA. Guess et al. [28,29] employed a similar approach to study the knee joint mechanics during gait using a 12DOF knee model with deformable contact for the estimation of TF forces during treadmill and normal gait. Both models used proportional-integrative-derivative (PID) feedback control gains to calculate muscle forces. Although these PID gains were modulated by the physiological cross-sectional area (PCSA) of each muscle, global gain values still needed to be set, for which no physiological tuning was available. A sensitivity analysis on the effect of the global control gains was performed by Guess et al. [28] and more accurate predictions were reported for smaller values of these gains. Hast and Piazza [30] proposed a "dual-joint" modeling approach consisting of an idealized knee joint-based inverse dynamics analysis for the estimation of muscle forces, followed by a forward-dynamics analysis using a 12DOF knee model with which contact forces were predicted using a rigid-body spring contact model. Despite the complexity of their model, no effort was made to scale the MS architecture to the patient. The reader is referred to the review paper by Erdemir et al. [9] for an extensive review on MS modeling and optimization techniques for estimation of muscle forces in vivo.

Andersen and Rasmussen [31] have proposed an enhanced inverse dynamics approach, called force dependent kinematics, which simultaneously computes the internal forces and secondary joint kinematics. This is accomplished by assuming that the secondary knee DOFs are not influenced by the global model dynamics and can, therefore, be solved assuming quasi-static equilibrium between ligament, muscle, contact forces, and external loads. Hence, the application of this FDK technique enables the simulation of the knee joint mechanics in a much more realistic manner than simulating the knee joint with idealized constraints.

Accurate representation of the MS model architecture is also essential for obtaining reliable subject-specific model predictions [32,33]. New advanced scaling techniques, such as morphing, have emerged, which allow better scaling of MS models to the subject-specific anatomy than techniques based on linear scaling laws [34,35]. However, none of the recent MS modeling methodologies have made an effort to integrate a subject-specific anatomical representation of the MS architecture together with a detailed representation of the knee joint.

The specific aims of the present study, hence, are (a) to develop an MS modeling framework based on subject-specific computed tomography (CT) images, motion capture data, and force plate data, which is capable of estimating in vivo ligament and muscle forces, TF contact forces, and knee joint kinematics; (b) to evaluate the validity of the TF joint force and secondary knee kinematic predictions based on the experimental data available in the fifth grand challenge competition dataset; and (c) to assess the influence of knee modeling approach (idealized hinge versus FDK representation) on the knee model on the predicted outcome variables.

Materials and Methods

Experimental Data. The data used in this study were part of the fifth grand challenge dataset for the 7th World Congress of Biomechanics (July 6–11, 2014, Boston, MA) [8].[1] The data were obtained from one male subject (age—86, height—180 cm, and BW—75 kg), who received a posterior cruciate-retaining (PCR) total knee replacement (TKR) of his left knee. The tibial implant, a generation II tray design (eTibia), was equipped with a telemetric force-measuring sensor that measured the six load components transferred through the prosthesis [6,36]. The competition data included eTibia loads, trajectories of motion capture markers, force plate data, EMG for a series of gait trials, joint calibration trials and fluoroscopy trials, and pre- and postoperative CT data. Geometric stereolithography (STL) 3D geometries of the prostheses were provided for the femoral component, tibial tray and insert, patellar button, along with postoperative bone geometries of partial pelvis, femur, patella, tibia, fibula, partial talus, and partial calcaneus.

MS Model

Full-Body Model. A subject-specific MS model was developed using the anybody modeling system (AMS) version 6.0.2 (Anybody Technology A/S, Aalborg, Denmark), a software for the simulation and analysis of the MS system [37]. The generic human body model from the AnyBody Managed Model Repository (AMMR) version 1.6 was the basis for the subsequent personalization with the subject-specific data. It comprises head, two arms, trunk, pelvis, and two legs. The leg model was updated to the newly collected Twente Lower Extremity Model version 2.0 (TLEM 2.0) dataset [38] based on clinical images and comprises thigh, shank, patella, talus, and foot segments, together with coordinates of all muscle attachments and wrapping shapes. Segments were connected to each other by means of hinge joints at the neck, ankle, subtalar, TF, and PF joints, and by means of spherical joints at the glenohumeral and hip joint, and between the vertebrae of the lumber spine in addition to a spinal rhythm that leaves three DOFs between pelvis and thorax. A more complex representation of the TF and PF joints was also used in this study, in which the constraints of the hinge joints were released, leaving additional DOFs to be controlled. We will describe this in more detail in

[1] https://simtk.org/home/kneeloads

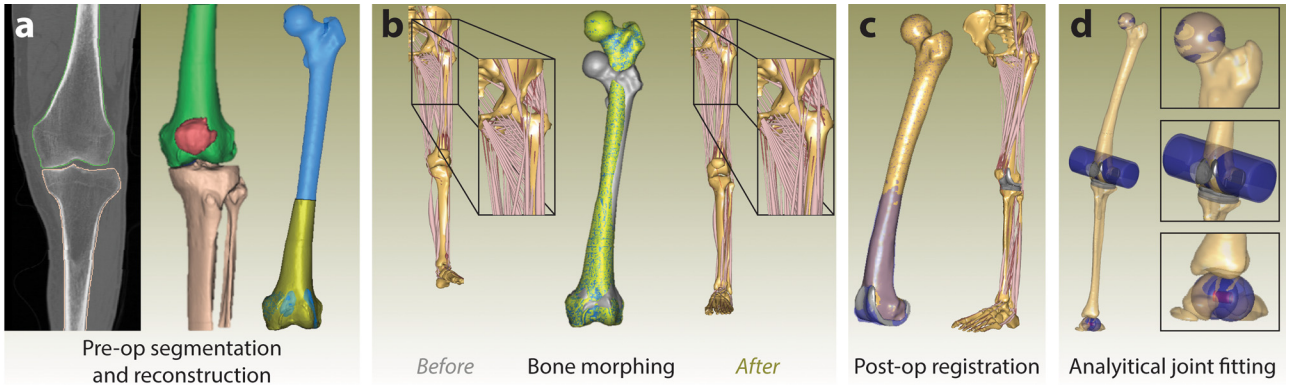

Fig. 1 Steps for obtaining a subject-specific MS model. (*a*) Pre-operative bone segmentation from CT images. Partial bones were merged with postoperative bone geometries to generate complete 3D pre-operative bone models, (*b*) morphing of the generic TLEM 2.0 bone meshes to the patient-specific pre-operative bones (note the variation in muscle insertion sites), (*c*) registration of postoperative bone geometries to the morphed pre-operative bones, (*d*) analytical joint fitting of postoperative bone geometries to obtain patient-specific hip joint center, TF, PF, ankle, and subtalar joint axes.

section FDK Model. Fifty-five muscle–tendon (MT) units were represented using 166 Hill-type one-dimensional string elements spanning from origin to insertion through via-points and wrapping over analytical surfaces fitted to the bone geometries.

Model Scaling. To scale the TLEM 2.0 generic model to the subject-specific bone geometries, we segmented the subject's pre-operative bone CT images in Mimics version 14 (Materialise NV, Leuven, Belgium), and 3D bone geometries were exported in the STL format (Fig. 1(*a*)). Only the distal femur and proximal tibia–fibula were available in the pre-operative CT images. Thus, these partial 3D bone models were combined with postoperative full-leg 3D bone models provided in the dataset to obtain complete pre-operative bone models. An advanced morphing method, based on the 3D reconstruction system of Redert et al. [34], developed by Materialise NV (Leuven, Belgium) and evaluated by Pellikaan et al. [35], morphed the topology of the TLEM 2.0 atlas bones to the corresponding subject-specific pre-operative bones (Fig. 1(*b*)). These morphed bone meshes were used to scale the muscle attachment sites defined on the given segment using a radial basis function (RBF) interpolation scheme: First, an affine transformation was defined to roughly scale the original TLEM 2.0 generic bone (source) to the subject-specifically morphed TLEM 2.0 bone (target) based on selected bony landmarks; second, a triharmonic RBF scaling function was defined based on the vertices of the above affine-transformed TLEM 2.0 bone geometry and the subject-specifically morphed TLEM 2.0 bone geometry using the available facility in the AMS. To avoid the poor extrapolation properties of RBF functions, corners of a bounding box defined around each bone were included in the mapping. Finally, a reverse rigid-body transformation was defined based on the previously used bony landmarks to bring the morphed MS geometry back from the CT reference frame to the body model reference frame in the AMS. Geometry-based morphing was impossible for the talus due to an incomplete CT scan. Therefore, talus was morphed with an affine transformation based on selected bony landmarks only. After morphing, the postoperative geometry files, including the prosthesis, were aligned with the pre-operative geometries using a rigid-body registration (Fig. 1(*c*)) to provide the subject-specific postoperative geometrical model.

To obtain accurate joint centers and axes, we performed analytical surface fits on the postoperative bones (Fig. 1(*d*)): The hip joint center was determined through a spherical fit to the femoral head, the TF, and PF joint axes by fitting two different cylindrical surfaces around the femoral component, and the talocrural joint axis by fitting two spherical surfaces to talus [39].

Since the CT scan did not include all bones in the model, a different approach had to be taken for the scaling of the remaining segments. For the bones morphed above, we assumed symmetry between the left and right legs. To scale the length of the remaining upper body segments, the pelvic bone width, and the foot lengths, a nonlinear least-square optimization problem was defined using a linear segment scaling law [40]. This optimization problem minimized the difference between model markers and experimentally recorded marker positions during one frame of a standing reference trial (PS_staticfor2), using the method of Andersen et al. [41], while enforcing the idealized joint constraints. Skin markers were placed directly on bony landmarks and the shoe of the subject was manually placed on the MS model at the estimated corresponding locations. After the optimization of the segment lengths, the local coordinates of all markers in clusters placed on the thigh and shank were computed in the segment reference frames and saved in files together with the optimal segment lengths for later use.

Muscle Model and Strength Scaling. Muscle dynamics was defined by three-element Hill type models as proposed by Zajac [42]. Each MT unit in the TLEM 2.0 dataset was assigned an isometric muscle strength, F_0, calculated by multiplying the PCSA by a factor of 27 N/cm^2. The PCSA was derived from a cadaver-based muscle volume divided by the optimum fiber length. Force–length and force–velocity relations were included in the definition of muscle strength to account for the length- and velocity-dependent effect on the instantaneous muscle strength. Tendon slack lengths were calibrated using dedicated calibration routines included in the TLEM 2.0 leg model.

A length–mass scaling approach was employed to scale the muscle strength of the standard TLEM 2.0 model to the specific subject of interest, using a method originally proposed by Rasmussen et al. [40]. Specifically, the isometric muscle strength of each muscle unit was scaled using segment-specific strength scaling factors based on the length and mass of the segment relative to the generic TLEM 2.0 model.

A reduced strength of the flexor/extensor muscles has been reported for patients who undergo TKA [43], which could be quantified in a 31% reduction of the isometric flexion/extension peak torque, on average, but with reductions of up to 40% at low flexion angles. Consequently, all muscles involved in flexion/extension in the model were affected by a reduction of 35% of their nominal PCSA and, hence, their strength. Ideally, the subject-specific muscle strength should have been scaled based on direct measurement of lower extremity maximal joint torques. Unfortunately, the strength reductions applied could not be verified as strength measurements were not available for this subject.

Muscle Recruitment Problem. The muscle recruitment problem was solved by minimizing a polynomial cost function G

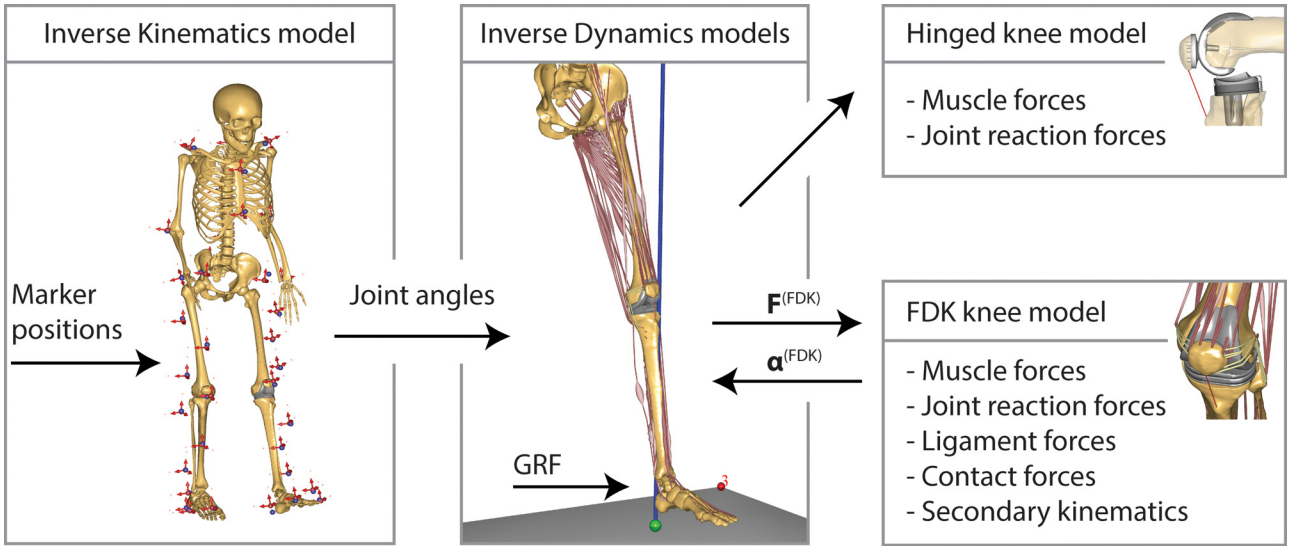

Fig. 2 Simplified schematic of the modeling workflow. Marker trajectories are input to an inverse kinematics-based analysis that computes joint angles. Inverse dynamics like models are developed, in which GRFs are input together with joint angles. Two types of knee models are simulated: A hinged model and an FDK model. The hinged model employed idealized constraints, whereas the FDK model finds a quasi-static kinematic configuration, $\alpha^{(FDK)}$, in the FDK DOFs under the influence of the forces, $F^{(FDK)}$, acting in the respective DOFs. Predictions are independently produced by each model. The FDK model provides, in addition to muscle forces and joint reactions, also ligament and contact forces, and secondary knee kinematics.

(Eq. 1(*a*)), subject to the equilibrium equations (1(*b*)) and to the constraint that muscles can only pull and cannot generate a force larger than the instantaneous strength (1(*c*)), as described in Ref. [44]. In the TLEM 2.0, muscles with a wide origin/insertion area were split into multiple branches. However, as shown by Holmberg and Klarbring [45], such a subdivision of muscles affects the muscle and joint reaction force estimates. Consequently, a normalization factor based on the muscle volume was introduced, according to Ref. [46], which accounts for a proper subdivision of the force among split and nonsplit muscles

$$G(\mathbf{f}^{(\mathrm{M})}) = \sum_{i=1}^{n^{(\mathrm{M})}} V_i \left(\frac{f_i^{(\mathrm{M})}}{N_i} \right)^3 \tag{1a}$$

$$\mathbf{Cf}=\mathbf{d} \tag{1b}$$

$$0 \le f_i^{(\mathrm{M})} \le N_i, \quad i = 1, \ldots, n^{(\mathrm{M})} \tag{1c}$$

where G is the cost function to minimize, M indicates the muscles, and $\mathbf{f}^{(\mathrm{M})}$ is the vector of the $n^{(\mathrm{M})}$ unknown muscle forces. More precisely, $n^{(\mathrm{M})}$ is the number of all muscle units after the geometrical splitting, $f_i^{(\mathrm{M})}$ denotes the individual ith muscle force, and N_i is the instantaneous muscle strength, depending on the current working conditions of the Hill-type model, namely, the force–length and force–velocity relationships. $\mathbf{C}$ is a coefficient matrix for all the unknown forces in the problem, $\mathbf{f}$, which includes joint reactions as well as muscle forces, and $\mathbf{d}$ contains all the external loads and inertia forces. Finally, V_i is the volume of each muscle unit and, for split muscles, each unit was assigned the corresponding fraction of the total muscle volume resulting from a uniform subdivision by the number of units. The muscle volume was computed as the product of PCSA and optimum fiber length, taking into account the reduction in PCSA for all knee flexors and extensors.

Marker-Tracking and Inverse Dynamics. With the model scaled, an inverse kinematics technique [47] was employed to track the marker trajectories during one normal gait (PS_ngait_og_ss1) and one right-turn (PS_rightturn6) trial from the grand challenge competition dataset (Fig. 2), providing the time history of the following body kinematics: One neck rotation, three pelvis–thorax rotations, three pelvis translations and three rotations, three hip rotations, knee flexion angle, ankle plantarflexion, and subtalar eversion. During the marker-tracking stage, all joints were assumed idealized and the TF and PF joints were modeled as hinges (i.e., revolute joints), allowing only one rotational DOF (flexion/extension) around a fixed joint axes. Inaccuracies in the estimation of knee joint kinematics from marker data due to soft tissue artifacts (STA) have been reported [48], and the use of knee joint constraints did not result in a reduction of STA [49]. From these observations derived the choice of using hinge joint constraints for the knee and to drive only the knee flexion angle from marker data in the FDK model as explained later. The PF joint was further constrained by enforcing a fixed-length patellar ligament. This model did not include ligaments or contact but idealized constraints, as is typically the case when an idealized hinge joint is used to model the knee. We will refer to this as the hinged knee model.

Joint angles and ground reaction forces (GRFs) were input to the inverse dynamic analyses with the hinged knee model. Only the left lower extremity, trunk, and head dynamics were simulated, and six residual forces and moments were inserted at the pelvis. Muscle and joint reaction forces were the outputs of these types of simulations.

FDK Model. A second model containing a total of 11 knee DOFs, rigid–rigid contact, and ligaments was developed (Fig. 3) and solved using the FDK solver in the AMS (we will refer to this as the FDK knee model). All the TF and PF joint constraints were released, leaving six DOFs in the TF joint and five DOFs in the PF joint, as the patellar ligament was still considered rigid. Similar to the hinged model, the knee flexion angle was the only knee DOF to be driven from marker data, whereas the other five TF and five PF DOFs were left free to equilibrate under the effect of external loads, muscle, ligament, and contact forces, which were simultaneously computed using FDK, an enhanced inverse dynamics-based method in the AMS [50]. In summary, the FDK solver perturbed the kinematic configuration along the FDK DOFs ($\boldsymbol{\alpha}^{(FDK)}$) until a quasi-static equilibrium was found, in which all the FDK residual forces ($\mathbf{F}^{(FDK)}$) in these DOFs were zero (Fig. 2). Any dynamic effects in those 10 DOFs were neglected and quasi-static equilibrium at every simulation step was

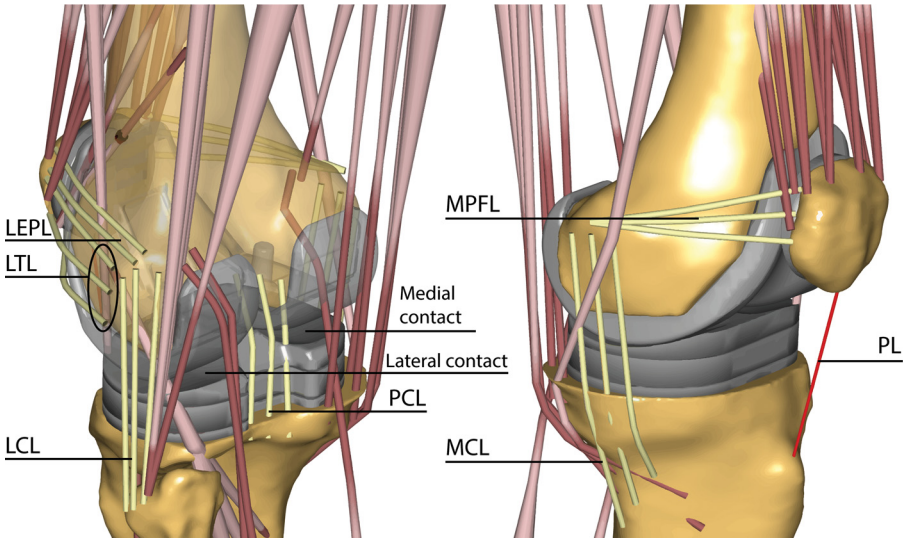

Fig. 3 The 11-DOF knee model used in the FDK simulations. Knee flexion is driven using joint angle from an inverse kinematic-based analysis. The remaining 10DOFs are handled by the FDK solver. Ligaments are modeled as one-dimensional string elements wrapping around geometrical shapes (abbreviations as described in the text). Medial and lateral contacts were modeled using rigid–rigid contact formulation. Patellar ligament (PL) consists of a rigid linkage between patella and tibia.

iteratively searched until force residuals fell below a specified threshold (=0.3 N). Please notice that, although quasi-static equilibrium in the secondary knee joint kinematics was assumed, all dynamics occurring due to knee flexion/extension was taken into account and, hence, only a small fraction of the overall knee dynamics was omitted.

Ligaments were included to provide stability to the unconstrained joints in the FDK model (Fig. 3). A total of 17 spring elements were modeled to represent the PCL (three bundles), medial collateral ligament (MCL, three bundles), lateral collateral ligament (LCL, three bundles), medial PF ligament (MPFL, three bundles), lateral epicondylopatellar ligament (LEPL, two bundles), and lateral transverse ligament (LTL, three bundles). Since attachment sites could not be determined from the dataset, they were estimated according to descriptions found in the literature [51–60]. The anterior cruciate ligament was sacrificed during the surgery and, therefore, not modeled. Force exerted by ligament bundles followed a nonlinear elastic characteristic with a slack region [61]

$$f(\varepsilon) = \begin{cases} \dfrac{k\varepsilon^2}{4\varepsilon_l}, & 0 \le \varepsilon \le 2\varepsilon_l \\ k(\varepsilon - \varepsilon_l), & \varepsilon > 2\varepsilon_l \\ 0, & \varepsilon < 0 \end{cases} \tag{2}$$

where $f(\varepsilon)$ is the current force, k is the stiffness, ε is the strain, and ε_l (= 0.03) is a constant related to the transition phase toward the linear region of the force–strain curve [62]. Ligament bundle slack length, l_0, was first calibrated in an upright reference position, in which the leg was fully extended, so that

$$l_0 = \frac{l_r}{\varepsilon_r + 1} \tag{3}$$

where l_r is the bundle length computed at the reference position and ε_r is the reference strain estimated for that reference position. Finally, the instantaneous strain, ε, during the simulation was computed from the instantaneous bundle length, l, as follows:

$$\varepsilon = \frac{l}{l_o} - 1 \tag{4}$$

Stiffness and reference strain assigned to each ligament bundles are summarized in Table 1. These values were adapted from the literature [61]. No direct information was available on the stiffness and slack length of medial (MPFL) and lateral (LEPL and LTL) PF ligaments. However, MPFL represents the major restraint to lateral patellar translation [55,63], whereas lateral structures only account for a lesser contribution. Thus, MPFL stiffness was chosen in the same range of other known ligaments (LCL and MCL), whereas lower values were assigned to LEPL and LTL bundles. Furthermore, medial retinacular structures are

Table 1 Stiffness and reference strains of the knee joint ligament bundles used in the FDK model

Ligament bundle[a]	Stiffness (N)[b]	Reference strain[c]
aPCL	6000	−0.24
mPCL	6000	−0.10
pPCL	6000	−0.03
aMCL	2750	0.04
mMCL	2750	0.04
pMCL	2750	−0.03
aLCL	2000	−0.25
mLCL	2000	−0.05
pLCL	2000	0.08
sMPFL	2000	0.12
mMPFL	2000	0.08
iMPFL	2000	0.08
sLEPL	1000	0.06
iLEPL	1000	0.06
sLTL	1000	0.06
mLTL	1000	0.06
iLTL	1000	0.06
PL	∞	—

[a]aPCL/mPCL/pPCL, anterolateral, middle, and posteromedial cruciate ligament; aMCL/mMCL/pMCL, anterior, middle, and posterior medial collateral ligament; aLCL/mLCL/pLCL, anterior, middle, and posterior lateral collateral ligament; sMPFL/mMPFL/iMPFL, superio, middle, and inferior medial patellofemoral ligament; sLEPL/iLEPL, superior, and inferior epicondylopatellar ligament; sLTL/mLTL/iLTL, superior, middle, and inferior lateral transverse ligament; PL, patellar ligament.
[b]Stiffness is expressed in Newton per unit strain.
[c]Reference strains are referred to an upright standing reference position.

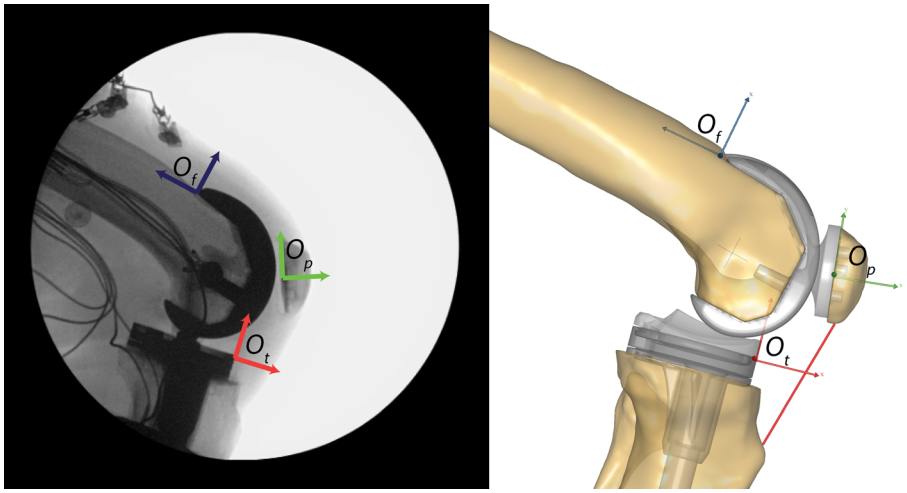

Fig. 4 Reference frames used to express the knee planar knee kinematics during the leg-swing trial in the fluoroscopy images (left) and in the MS model (right). The PF flexion is defined as the rotation of the femoral frame (O_f) relative to the patellar frame (O_p); PT flexion is the rotation of the tibial frame (O_t) relative to the patellar frame; TF tip and PT shift are given by the two coordinates of displacement (posterior–anterior and distal–proximal) of femoral frame and patellar frame, respectively, relative to the tibial frame. Muscles are hidden in the model view and the hinged model version is shown.

tight during knee extension to low flexion angles and relax with increased flexion [60]; hence, MPFL, LPL, and LTL reference strains were assigned similar positive values, providing the required stability to the PF joint. The choice of parameters was evaluated to ensure that the patellar button always ran into the groove of the femoral component during a test flexion/extension simulation. The patellar ligament was modeled as a rigid one-bundle linkage between patella and tibia in both the hinge and FDK models, and its length was estimated based on measurements from fluoroscopy images with the subject performing a leg-swing trial, as described later. Similar to the muscle models, wrapping surfaces were employed to prevent ligaments from penetrating the bones and the implants. Specifically, one cylinder was positioned medially on the distal femur so that the MPFL bundles could wrap around the medial condyle of the femur. Another cylinder was placed on the contralateral side so that LEPL and LTL bundles would wrap around the lateral femur condyle. A third cylinder ensured that the PCL bundles did not penetrate the spine structure of the tibial insert. Finally, one cylinder was positioned on the tibial segment to allow the MCL to wrap around the medial tibial condyle.

A rigid–rigid STL-based contact model was defined between tibial insert and femoral component and between the patellar button and the femoral component. Contact forces were computed based on linear volume approximations using the penetration depth, d_i, of a vertex of one triangle-mesh into the closest triangle of the opponent STL surface. A volume, V_i, was approximated by multiplying the vertex penetration depth by the opponent triangle area, A_i, so that for the ith vertex

$$V_i = A_i d_i \tag{5}$$

The contact force magnitude for an element that contributed to the total contact force was computed using a linear relationship between the penetration volume and a so-called pressure module, P

$$F_i = PV_i \tag{6}$$

The direction of the force was determined by the normal of the triangle. Based on previous tests, for all contact pairs, a pressure module of 9.3 GN/m^3 was used. This value provided a good trade-off between the amount of penetration obtained and the numerical issues involved in solving contact between two surfaces with high stiffness. Three contact models of the kind described above were defined, one for the medial side, one for the lateral side of the TF joint, and one for the PF joint. The forces computed from the two TF contact models where expressed in the reference frame of the tibial component, thus permitting a direct comparison with the measured knee loads provided with the grand challenge dataset. Finally, linear and rotational springs with small stiffness values were included at each of the ten FDK DOFs in the FDK knee model, which served exclusively to help the FDK algorithm in searching the static equilibrium among those DOFs by ensuring that there was always stiffness in the model, even if the solver explored nonphysiological configurations. The stiffness of these springs did not need to be tuned, and care was taken that the spring forces remained negligible once the solution had been found.

The time history of joint angles and GRFs was input to the FDK analyses. Only the left lower extremity, trunk, and head dynamics were simulated, and six residual forces and moments were inserted at the pelvis. Muscle, ligament, contact, and joint reaction forces along with secondary knee kinematics were the outputs of the FDK simulations (Fig. 2).

Estimation of Secondary Knee Kinematics. An unloaded leg-swing fluoroscopy trial (PS_legswing2) from the dataset was used to obtain an estimate of knee kinematics in the sagittal plane, namely, TF and PF translations, PF, and patellotibial (PT) flexion angles. During the trial, the subject performed a knee flexion–extension movement with his left leg while standing on the other (right) leg. The left knee was imaged through an X-ray fluoroscope at a frame rate of 30 images per second. Twenty-seven fluoroscopic images from the trial were segmented using custom code written in MATLAB version 8.1.0 (The Mathworks, Inc., Natick, MA). The available range of motion for these images spanned from approximately 100 deg–30 deg of knee flexion. The pixel size was determined by manually registering the 3D geometric model of the femoral component (with known dimensions) to one fluoroscopy frame. Relative angles and displacements between patella, femoral, and tibial component projections were detected using edge- and line-detection routines based on the Hough transform. The trajectories of the superior tip of the femoral

component (TF tip shift) and of the patella (PT shift) were expressed relatively to a reference frame placed on the extreme anterior edge of the tibial tray, as depicted in Fig. 4. The same local frames were defined in the hinge and FDK models allowing a direct comparison between fluoroscopy-detected and model-predicted kinematics.

The fluoroscopy-detected TF flexion was used to drive the knee flexion angle in the inverse dynamic and FDK simulations. Hip and ankle rotations were not directly available, and they were visually estimated from a movie recorded while the subject was performing the task. The distance between the inferior tip of the patella and the tibial tuberosity was manually measured in all fluoroscopy frames. The mean value was used as an estimate of subject-specific patellar ligament length for both hinge and FDK models.

No fluoroscopy data were available for the gait and right-turn trials and, therefore, only the unloaded leg-swing fluoroscopy trial was used for the evaluation of secondary knee kinematics.

Model Evaluation. TF joint compressive contact forces were estimated with both the hinged model and the FDK model during a gait trial and a right-turn trial, leading to four different simulations. Predictions were expressed as fractions of BW and resampled on a 0–100% trial duration scale with a step interval of 1% from heel strike to the subsequent heel strike. Medial and lateral TF joint forces were obtained from the hinged model using regression equations provided in the grand challenge competition dataset, whereas in the FDK model, they were independently computed from the two separate medial and lateral contact models. Ligament forces predicted by the FDK model are also reported for the gait and right-turn trials.

Knee kinematics during the leg-swing fluoroscopy trial was estimated with both the hinge and the FDK knee models, leading to two additional analyses. Model-predicted and fluoroscopy-detected results were resampled to a 0–100% trial duration scale with a step interval of 1%.

Differences between model predictions and experimental measurements were quantified in terms of RMSE, squared Pearson correlation coefficient (r^2), coefficient of determination (R^2), and the Sprague and Geers metrics of magnitude (M), phase (P), and combined error (C) [64,65]. Sprague and Geers metrics can quantify magnitude and phase prediction errors independently and they are both zero when the compared curves are identical; C combines the two errors and was computed as the root of the sum of squares of M and P.

Results

TF Joint Forces. Predicted versus experimental TF contact forces during the gait and right-turn trials are depicted in Fig. 5. Experimental data from the instrumented knee implant revealed a double-peaked total force during the gait cycle, with a first peak of 2.2 BW occurring at the beginning of stance, and a second peak of 2.1 BW occurring toward the end of the stance phase. Both the hinge and FDK knee model captured this pattern ($R^2 = 0.9$, RMSE < 0.3 BW) and predicted the first and second peaks equal to 2.0 and 2.4 BW, respectively. Lateral forces were in general underpredicted by both the hinged model ($M = -0.3$) and the FDK model ($M = -0.4$), and a considerable phase error was observed ($P = 0.2$). Medial forces were slightly overpredicted by both models ($M = 0.1$). Right-turn total forces were in overall good agreement with the experimental forces (RMSE = 0.3 BW), as predicted by both hinge model ($R^2 = 0.8$) and FDK model ($R^2 = 0.9$) simulations; moderate medial side force underprediction ($M = -0.3$) and lateral side overprediction ($M = 0.2$) were observed. Both FDK and hinged model captured the overall shape and timing of the measured TF contact forces (Table 2).

Ligament forces during the gait and right-turn trial predicted with the FDK model are depicted in Fig. 6. The PCL was moderately stretched right after toe-off during the gait (respectively right-turn) trial, when knee flexion angle was approximately 60 deg, with a peak force of 68 N (respectively 62 N). The MPFL, MCL, and LEPL generated the most considerable force throughout both cycles. Mean forces predicted were 88 N, 43 N, 55 N, respectively, in the gait trial simulation and were 87 N, 48 N, 47 N, respectively, in the right-turn trial simulation. The predicted LCL force was less than 30 N throughout the cycle in both trials.

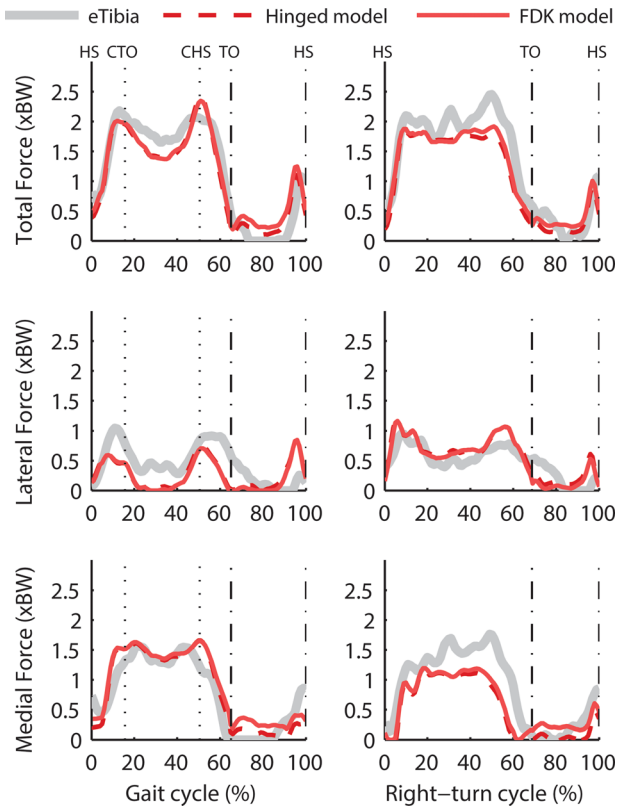

Fig. 5 Total, lateral and medial compressive TF contact forces predicted during one gait trial (left column) and one right-turn trial (right column) using an idealized knee joint model and the FDK knee model. Experimental measurements are reported for the same trial. Overall good agreement between measured and predicted total forces is noted. Lateral (respectively medial) forces are slightly underpredicted (respectively overpredicted) in the gait trial. Lateral (respectively medial) forces are slightly overpredicted (respectively underpredicted) in the right-turn trial.

Secondary Knee Kinematics. The experimental PF and PT flexion curves during the unloaded leg-swing fluoroscopy trial were almost linear relative to the knee flexion angle and spanned from approximately 74–20 deg and 25–9 deg, respectively, from flexion to extension (Fig. 7, left). The PF flexion was perfectly predicted by the FDK model ($R^2 = 0.99$), and the hinged model resulted in a larger prediction error ($M = 0.26$, $R^2 = 0.52$) with respect to the experimental curve. The PT flexion was also much better predicted using the FDK model ($R^2 = 0.7$) than using the hinged model ($R^2 < 0$), as explained by the larger magnitude error in the hinged model prediction ($M = -0.75$). The posterior–anterior TF tip shift (Fig. 7, top right) was overall well predicted by both the hinged model ($R^2 = 0.88$) and the FDK model ($R^2 = 0.96$), whereas the distal–proximal TF tip shift was much better predicted by the FDK model ($R^2 = 0.96$) than by the hinged model ($R^2 = 0.38$). The hinged model failed almost completely at tracking the PT displacements (Fig. 7, bottom right), resulting in large combined errors. The FDK model predictions are better than

Table 2 Agreement between predicted and experimental TF joint compressive contact forces during gait and right-turn trials

	FDK knee model						Hinge knee model					
Trial	RMSE[a]	r^2	R^2	M	P	C	RMSE[a]	r^2	R^2	M	P	C
Gait												
Total force	0.26	0.90	0.89	−0.06	0.06	0.08	0.25	0.91	0.90	−0.07	0.05	0.09
Lateral force	0.35	0.23	−0.26	−0.35	0.22	0.41	0.34	0.21	−0.19	−0.31	0.21	0.38
Medial force	0.26	0.85	0.79	0.12	0.07	0.14	0.25	0.85	0.81	0.08	0.08	0.11
Right-turn												
Total force	0.29	0.94	0.87	−0.14	0.04	0.15	0.34	0.93	0.83	−0.17	0.05	0.18
Lateral force	0.21	0.65	0.33	0.17	0.10	0.20	0.21	0.64	0.32	0.21	0.10	0.23
Medial force	0.38	0.82	0.62	−0.29	0.08	0.30	0.44	0.83	0.48	−0.33	0.10	0.35

[a]RMSE is in units of BWs.

the ones from the hinged model with regards to the postero–anterior PT shift ($R^2 = 0.92$). However, the distal–proximal PT shift is systematically underpredicted ($M = -0.1$). Evaluation metrics for all the measures are summarized in Table 3. The average combined error for all the predictions from the FDK (respectively hinged) model was equal to 0.06 (respectively 0.34).

Discussion

The first goal of this study was to present an MS modeling framework based on subject-specific CT images, motion capture, and force plate data as input to an inverse dynamics-based method that concurrently predicts MS dynamics and detailed in vivo knee joint mechanics. Several aspects presented lend novelty and uniqueness to our MS modeling approach: The FDK method permitted the estimation of knee joint mechanics that also include contribution of soft tissues and contacts, while still employing motion capture and force plate data as the only information required to drive the model. A bone-morphing technique was employed to anatomically scale the generic MS architecture to the specific patient, including muscle attachment sites.

Our second aim was to evaluate the validity of the model predictions during walking activities performed by a subject with TKA using experimental data publicly available from the grand challenge competition [8]. Our models predicted TF contact forces which were in good agreement with the experimental measurements (RMSE < 0.3 BW during the gait trial). Previous models have predicted TF forces with an RMSE of 0.41 BW [29], 0.45 BW [66], and 0.67 BW [27] during gait. The time history and the value of peak contact forces were also identified with a good accuracy in both the gait and right-turn simulations (Fig. 5), with a maximum error of 0.3 BW on the second peak of stance during gait. Other authors have reported errors in peak value estimation up to 0.35 [28], 0.39 [27], 0.65 [66], and 0.80 BW [30], on average. We included the Sprague and Geers' metrics to evaluate the goodness of our model predictions, along with RMSE, squared Pearson's r (r^2), and coefficient of determination (R^2). Pearson's r^2 is usually good when the trends are overall captured even in presence of large magnitude errors; whereas the coefficient of

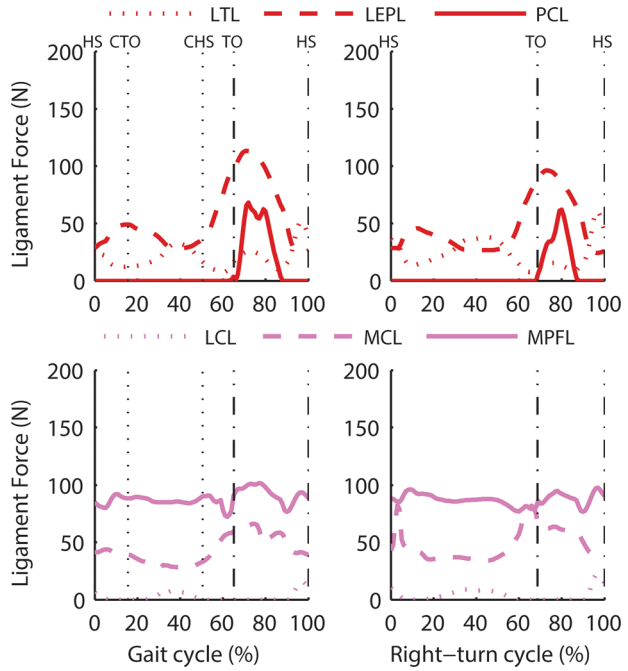

Fig. 6 Ligament forces predicted during gait (left) and right-turn (right) trials using the FDK model. Each force shown in the graphs was computed as the root of the summed squares of each ligament individual bundle force. The PCL is being activated after toe-off in both trials, and MPFL, MCL, and LEPL exert considerable amount of force throughout the trials.

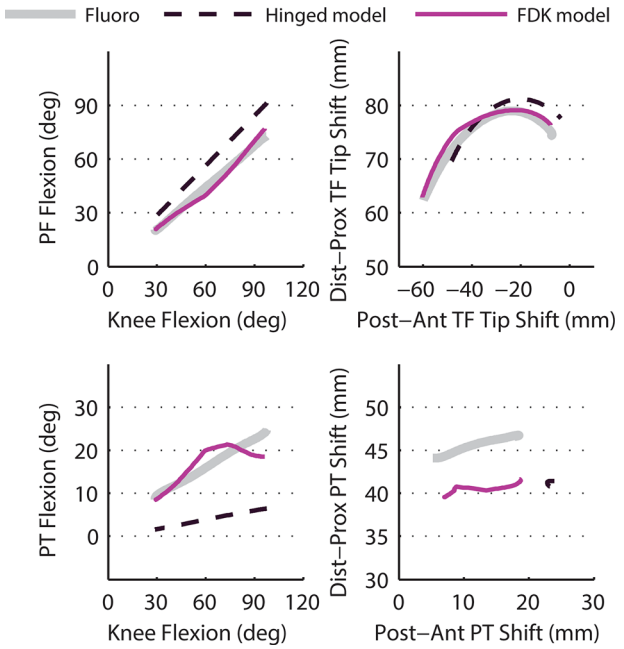

Fig. 7 Experimental versus predicted PF flexion (top left) and PT flexion (bottom left), plotted relative to knee flexion angle; TF tip shift (top right) and PT shift (bottom right). The FDK model predictions are generally more accurate than hinged model predictions. Note the inability of the hinged model to predict PT shifts, due to the absence of femoral roll-back.

Table 3 Agreement between predicted and detected secondary knee kinematics during unloaded leg-swing fluoroscopy trial

	FDK knee model						Hinge knee model					
Quantity[a]	RMSE[b]	r^2	R^2	M	P	C	RMSE[b]	r^2	R^2	M	P	C
PF flexion	2.33	0.99	0.99	0.00	0.02	0.02	13.3	1.00	0.52	0.26	0.01	0.26
PT flexion	3.05	0.71	0.70	−0.05	0.05	0.08	13.3	1.00	−4.83	−0.75	0.03	0.75
TF tip shift												
Posterior–anterior	3.69	0.99	0.96	0.07	0.02	0.08	6.79	1.00	0.88	−0.18	0.01	0.18
Distal–proximal	1.09	0.97	0.96	0.01	0.00	0.01	4.21	1.00	0.38	0.05	0.01	0.05
PT shift												
Posterior–anterior	1.32	0.93	0.92	−0.02	0.03	0.04	11.2	0.38	−4.79	0.69	0.11	0.70
Distal–proximal	5.19	0.85	−26.3	−0.11	0.00	0.11	4.57	1.00	−20.2	−0.10	0.01	0.10

[a]PF flexion, PF flexion; PT flexion, patellotibial flexion; TF tip shift, TF tip shift; PT shift, patellotibial shift.
[b]RMSE is in units of degrees for PF and PT flexion angles, and millimeters for TF and PT shifts.

determination, R^2, may results in low or even negative values in presence of magnitude errors or offsets even if the trends are well predicted. The interpretation of negative R^2 values is often difficult. Therefore, we believe that Sprague and Geers' metrics provide a more immediate way to quantify the magnitude and phase errors, especially when comparing time histories of quantities predicted by MS models and, therefore, their use should be encouraged.

The level of agreement of our results may also suggest that the criteria used for solving the muscle recruitment problem, as well as the muscle modeling and strength scaling applied, was able to approximate the particular MS biomechanics for this specific subject to a great extent. The over- or underpredictions of medial and lateral forces did not follow a particular trend, i.e., during the gait trial, the medial force was overpredicted, whereas in the right-turn, the lateral side was overpredicted, and vice versa. In general, the TF contact distribution is affected by the line of action of the GRF; during gait, it normally passes medially relative to the knee joint center resulting in a contact force more pronounced on the medial side [67]. The main contribution to support during walking is mainly given by muscle forces [68] and these, in turn, determine the forces exchanged at the joints. Therefore, the causes of the discrepancies between measured and predicted TF contact forces should be searched in the MS architecture of the model, including muscle strength, moment arms, and joint axes. The position of the lower extremity joints was not measured directly, and the foot model geometry could not be entirely reconstructed from medical images. The inevitable inaccuracies could have, therefore, resulted in small deviations in the predicted TF forces.

Estimates of ligament forces during the gait and right-turn trials were obtained using the FDK model. In a robotic in vitro study, Li et al. [69] measured the in situ force of PCL in CR-TKA and they observed that PCL force peaked at a knee flexion angle of 90 deg (39 ± 36 N). We predicted peak PCL forces of less than 70 N for both gait and right-turn trials, occurring right after toe-off at approximately 70% of the gait cycle, when the knee is flexed of about 60 deg. However, differences between the static setup used in the experiment and the dynamic nature of our simulations make this comparison questionable. Overall, predicted PCL forces compared qualitatively well with other model predictions in the literature. Thelen et al. [27] predicted a peak PCL force during gait of less than 200 N at about 70% of the gait cycle, whereas Kia et al. [29] predicted PCL peaks of about 100 N at approximately 50% of the gait cycle. Patterns of LCL and MCL forces agreed with those reported by Kia et al. [29] but differ from the ones of Thelen et al. [27].

As our third aim, we were interested in assessing whether a more complex representation of the knee joint substantially alters the model predictions. TF forces predicted using a hinged model formulation were generally comparable to the ones predicted by the FDK model (differences of less than 5% BW in RMSE of total force predictions). This reveals that using a different mechanical formulation for the knee joint, i.e., including more DOFs, did not substantially alter the load predictions at the tibial implant. Possible explanations for this are that the employed TKA implant is largely circular and a hinge joint is hence a good overall approximation of the knee joint structure, and the amount of knee motion predicted during the FDK simulations did not substantially alter the load distribution at the knee joint. The comparison against the fluoroscopic data does, however, reveal that the hinged model is less accurate at tracking the detailed joint kinematics compared to the FDK model, as revealed by the larger RMSE found for that model (Table 3). Whether this accuracy is sufficient depends on the application, but for instance for wear simulations, simultaneous estimates of contact forces as well as detailed joint kinematics are required. For such wear simulations, the FDK model should be preferred.

The ability to obtain subject-specific information on the conditions of the MS system is crucial if diagnostic information is to be carried out and interventions are to be planned based on the MS model outputs [8,9]. The approach presented was able to personalize a generic MS model to a great extent based on a vast amount of subject-specific information. Primarily, bones and muscle architecture of the subject's lower extremity were scaled using an advanced nonlinear morphing technique [35], from which derives that also all muscle attachments sites followed anatomical origin and insertion sites on the bony surfaces. This aspect is essential, since muscle forces are directly influenced by the line of action and moment arm during motion. No other studies did, to our knowledge, include a thorough and accurate anatomical representation of the MS architecture on a subject-specific body-scale level together with detailed models of the TF and PF joints. Several studies have used generic linear scaling law based on anthropometric information on the subject, i.e., BW, height, age, or gender [27–30,66]. Other studies have modified the anatomical description of the muscle architecture by including attachment sites taken from magnetic resonance imaging (MRI) scans from a different subject [70,71]. In our model, axes and joint centers of the lower extremity joints were extracted by fitting analytical geometrical shapes to the implant and bone geometries of the subject. Extracting the joint position from subject-specific images was recently proved to be a robust method in the frame of MS simulations [72].

Several studies have recently indicated the sensitivity of MT architecture in inverse dynamics-based simulations [66,73]. In this study, we have estimated the strength-related MT parameters by using linear scaling laws [40], in which length and mass of each segment served to further compute segment-specific strength coefficients. The knee flexor and extensor muscle strengths in our model were further decreased by 35% to account for weakening observed in the flexor–extensor mechanism in subjects following TKA [43]. To this regard, Hast and Piazza [30] predicted TF forces during gait with a forward-dynamic model of an elderly

subject, and they reduced uniformly by 50% all the muscle strength, to account for an age-related weakening of the MS system. Ideally, we could have included subject-specific strength in our model, if such information were made available.

Similarly to the model of Thelen et al. [27], we introduced a weighting factor in the objective function of the muscle recruitment problem, which accounted for the partial volume of the muscle branches. This was a major fundamental choice, considering the muscle architecture in our model. It has been shown that the estimated muscle forces in an inverse dynamics-based simulation are influenced by how the muscles are decomposed, to an extent that depends on the type of the recruitment criterion used and, particularly for polynomial criteria, on the power of the polynomial [45]. Many muscles in our lower extremity model were split to account for a large insertion area, while others were not. In particular cases, such as for soleus (split, three units) and gastrocnemius (not split), if no further normalization was introduced, the muscle recruitment problem would have seen it more favorable to activate gastrocnemius than soleus muscle (e.g., to plantar-flex the ankle). This is because the only gastrocnemius unit had a much larger strength compared to each of the three units of soleus. As this behavior was unwanted, muscle volume normalization factors were introduced in the objective function that accounted for the partial muscle volume of each individual muscle unit.

Although ligament forces were shown to contribute to only a minor extent to the TF contact forces [67], we have shown that they might instead have a larger influence in determining internal knee kinematics. In the simulation of leg-swing trial with the FDK knee model, TF and PF joint secondary sagittal plane kinematics were generally better approximated with FDK model simulations (Fig. 7), essentially because an unconstrained joint allowed motions that a hinge joint could not. In particular, the total absence of femoral roll-back when using the hinged model was most likely the cause of erroneous prediction of the PT kinematics. The FDK model, instead, could correctly predict the posterior–anterior displacement, but underpredicted the distal–proximal displacement. Therefore, although an overall agreement was reported, further studies are needed to determine whether ligament parameters used in the model are representative of a real situation, and it is likely that calibration routines will be required to fine-tune the joint restraint during the full range of knee flexion.

Simulations with the FDK model took approximately $4\frac{1}{2}$ h, for the gait and right-turn trial simulations, and $2\frac{3}{4}$ h for the leg-swing trial, respectively, to compute on a Windows 7, 64-bit 3.2 GHz Intel Core i5 processor, 16 GB RAM computer. The FDK residual forces were smaller than 1 N in the FDK simulations of right-turn and leg-swing trial and were smaller than 3 N in the gait trial simulation. Hinged model simulations required on average 2 min to complete. It should be emphasized that almost 90% of the time during an FDK analysis is spent on searching for the closest points during the contact force computation. This aspect should primarily be addressed in future studies for improving the computational speed of FDK simulations, for example, by utilizing surrogate modeling techniques [74].

This study includes some limitations that are worth discussing. First, we modeled the patellar ligament as a rigid linkage between patella and tibia. This may have slightly affected the predicted PCL strain, PF contact force, and TF kinematics during the knee range of motion [75]. However, the use of a stiff but extensible patellar ligament model needs to be investigated further. Second, the knee joint motions during the leg-swing fluoroscopy trial were detected for the quasi-sagittal fluoroscopy plane only. This might have introduced inaccuracies when evaluating the model-predicted sagittal plane kinematics, due to the presence of small out-of-plane motions. Furthermore, frontal and transversal plane PF and TF kinematics could not be evaluated with this method. Third, ligaments were modeled as one-dimensional nonlinear elastic springs, wrapping around geometrical shapes for preventing bone and implant penetration. This approach allowed large model simplifications but could not certainly grasp the complex stress-deformation characteristic of ligament tissue in 3D. In addition, tuning of the TF ligament properties was not performed for this subject, and the sensitivity of the corresponding ligament parameters on the model predictions was not assessed. We anticipate that knowledge of ligament insertion sites (for example, by MRI images of the subject's knee), in conjunction with laxity tests, could provide further calibration material for tuning the ligament parameters on a subject-specific basis. It is also worth mentioning that, although the effect of additional linear and rotational springs in the FDK model was negligible in the gait and right-turn trial simulations, contributions of up to 20 Nm were observed in the leg-swing trial FDK simulation at large flexion angles (approximately 70–100 deg). By removing the rotational spring at the tibial internal–external rotation FDK DOF, we understood that a large force was being recruited to restrain tibial external rotation at large flexion angles, and none of the modeled ligaments were able to support this motion, as both collateral ligaments were slack at high flexion. We concluded that the ligament configuration used in the model was not sufficient to completely stabilize the knee joint at large knee flexion angles. Further research will address a more detailed representation of the ligamentous restraint in the FDK knee model, we anticipate that the improvement of the popliteus complex representation on the posterolateral aspect of the knee might help further stabilizing the knee joint in flexion [76]. Fourth, time histories of predicted muscle activations were not evaluated, but their validity could be indirectly estimated through the evaluation of the joint forces. Notwithstanding the common practice of using EMG to validate muscle activations, muscle force production and EMG signal are two different physical phenomena related by complex mechanisms [42], and the EMG signal magnitude is location-dependent. Therefore, comparing EMG signal magnitude with model-predicted muscle activity cannot be regarded as the gold standard in assessing the validity of dynamic MS models. Also, the extent of leg muscle co-contraction was not evaluated in this study. The simultaneous activations of antagonistic muscles can result in increased joint forces [77], and this phenomenon can be regarded as physiological, to some extent, during load-bearing activities, as it may stiffen and further stabilize the joints. Considering the use of a purely muscle activity minimizing criterion for solving the muscle recruitment problem, it is likely that muscle co-contraction was underestimated in our models.

In conclusion, we have presented a novel multibody dynamics framework for the study of the MS system capable of directly integrating subject-specific clinical images, motion capture data and GRFs, for simultaneously predicting internal TF forces and secondary knee kinematics in vivo. We compared our model predictions to publicly accessible experimental data from a TKA patient, and found distinctly good agreement. Compared to use of a hinge knee model, use of more complex FDK TF and PF models did not result in improved prediction of knee contact forces but did result in more accurate prediction of secondary knee kinematics. The proposed workflow for developing subject-specific models may have potential application as a diagnostic tool and in aiding clinical decision-making.

Acknowledgment

We wish to thank B. J. Fregly, Ph.D., D. D. D'Lima, MD, Ph.D. and colleagues as the organizers of the fifth "Grand Challenge Competition to Predict in vivo Knee Loads" for making such invaluable experimental data publicly available. This study was supported by the "TLEM*safe*" project, funded by the Seventh Framework Programme of the European Union, and by the "BioMechTools" project, funded by the European Research Council.

References

[1] Westerhoff, P., Graichen, F., Bender, A., Rohlmann, A., and Bergmann, G., 2009, "An Instrumented Implant for In Vivo Measurement of Contact Forces and Contact Moments in the Shoulder Joint," Med. Eng. Phys., **31**(2), pp. 207–213.

[2] Bergmann, G., Graichen, F., Bender, A., Kääb, M., Rohlmann, A., and Westerhoff, P., 2007, "In Vivo Glenohumeral Contact Forces-Measurements in the First Patient 7 Months Postoperatively," J. Biomech., **40**(10), pp. 2139–2149.
[3] D'Lima, D. D., Fregly, B. J., Patil, S., Steklov, N., and Colwell, C. W., 2012, "Knee Joint Forces: Prediction, Measurement, and Significance," Proc. Inst. Mech. Eng., Part H, **226**(2), pp. 95–102.
[4] Bergmann, G., Deuretzbacher, G., Heller, M., Graichen, F., Rohlmann, A., Strauss, J., and Duda, G. N., 2001, "Hip Contact Forces and Gait Patterns From Routine Activities," J. Biomech., **34**(7), pp. 859–871.
[5] Damm, P., Graichen, F., Rohlmann, A., Bender, A., and Bergmann, G., 2010, "Total Hip Joint Prosthesis for In Vivo Measurement of Forces and Moments," Med. Eng. Phys., **32**(1), pp. 95–100.
[6] D'Lima, D. D., Townsend, C. P., Arms, S. W., Morris, B. A., and Colwell, C. W., 2005, "An Implantable Telemetry Device to Measure Intra-Articular Tibial Forces," J. Biomech., **38**(2), pp. 299–304.
[7] Bergmann, G., 2008, "Orthoload.com," Charité Univ. Berlin, http://www.orthoload.com/?page_id=7
[8] Fregly, B. J., Besier, T. F., Lloyd, D. G., Delp, S. L., Banks, S. A., Pandy, M. G., and D'Lima, D. D., 2012, "Grand Challenge Competition to Predict In Vivo Knee Loads," J. Orthop. Res., **30**(4), pp. 503–513.
[9] Erdemir, A., McLean, S., Herzog, W., and van den Bogert, A. J., 2007, "Model-Based Estimation of Muscle Forces Exerted During Movements," Clin. Biomech. (Bristol, Avon), **22**(2), pp. 131–154.
[10] Goislard de Monsabert, B., Vigouroux, L., Bendahan, D., and Berton, E., 2014, "Quantification of Finger Joint Loadings Using Musculoskeletal Modelling Clarifies Mechanical Risk Factors of Hand Osteoarthritis," Med. Eng. Phys., **36**(2), pp. 177–184.
[11] Mellon, S. J., Grammatopoulos, G., Andersen, M. S., Pegg, E. C., Pandit, H. G., Murray, D. W., and Gill, H. S., 2013, "Individual Motion Patterns During Gait and Sit-to-Stand Contribute to Edge-Loading Risk in Metal-on-Metal Hip Resurfacing," Proc. Inst. Mech. Eng., Part H, **227**(7), pp. 799–810.
[12] Lemieux, P.-O., Nuño, N., Hagemeister, N., and Tétreault, P., 2012, "Mechanical Analysis of Cuff Tear Arthropathy During Multiplanar Elevation With the AnyBody Shoulder Model," Clin. Biomech. (Bristol, Avon), **27**(8), pp. 801–816.
[13] Lemieux, P. O., Tétreault, P., Hagemeister, N., and Nuño, N., 2013, "Influence of Prosthetic Humeral Head Size and Medial Offset on the Mechanics of the Shoulder With Cuff Tear Arthropathy: A Numerical Study," J. Biomech., **46**(4), pp. 806–812.
[14] Weber, T., Dendorfer, S., Dullien, S., Grifka, J., Verkerke, G. J., and Renkawitz, T., 2012, "Measuring Functional Outcome After Total Hip Replacement With Subject-Specific Hip Joint Loading," Proc. Inst. Mech. Eng., Part H, **226**(12), pp. 939–946.
[15] Weber, T., Al-Munajjed, A. A., Verkerke, G. J., Dendorfer, S., and Renkawitz, T., 2014, "Influence of Minimally Invasive Total Hip Replacement on Hip Reaction Forces and Their Orientations," J. Orthop. Res., **32**(12), pp. 1680–1687.
[16] Grujicic, M., Pandurangan, B., Xie, X., Gramopadhye, A. K., Wagner, D., and Ozen, M., 2010, "Musculoskeletal Computational Analysis of the Influence of Car-Seat Design/Adjustments on Long-Distance Driving Fatigue," Int. J. Ind. Ergon., **40**(3), pp. 345–355.
[17] Rasmussen, J., Tørholm, S., and de Zee, M., 2009, "Computational Analysis of the Influence of Seat Pan Inclination and Friction on Muscle Activity and Spinal Joint Forces," Int. J. Ind. Ergon., **39**(1), pp. 52–57.
[18] Mirakhorlo, M., Azghani, M. R., and Kahrizi, S., 2014, "Validation of a Musculoskeletal Model of Lifting and Its Application for Biomechanical Evaluation of Lifting Techniques," J. Res. Health Sci., **14**(1), pp. 23–28.
[19] Kinney, A. L., Besier, T. F., Silder, A., Delp, S. L., D'Lima, D. D., and Fregly, B. J., 2013, "Changes in In Vivo Knee Contact Forces Through Gait Modification," J. Orthop. Res., **31**(3), pp. 434–440.
[20] Zelle, J., Heesterbeek, P. J. C., De Waal Malefijt, M., and Verdonschot, N., 2010, "Numerical Analysis of Variations in Posterior Cruciate Ligament Properties and Balancing Techniques on Total Knee Arthroplasty Loading," Med. Eng. Phys., **32**(7), pp. 700–707.
[21] Mootanah, R., Imhauser, C. W., Reisse, F., Carpanen, D., Walker, R. W., Koff, M. F., Lenhoff, M. W., Rozbruch, S. R., Fragomen, A. T., Dewan, Z., Kirane, Y. M., Cheah, K., Dowell, J. K., and Hillstrom, H. J., 2014, "Development and Validation of a Computational Model of the Knee Joint for the Evaluation of Surgical Treatments for Osteoarthritis," Comput. Methods Biomech. Biomed. Eng., **17**(13), pp. 1502–1517.
[22] Van Duren, B., Pandit, H., Murray, D., and Gill, H., 2014, "Approximation of the Functional Kinematics of Posterior Stabilised Total Knee Replacements Using a Two-Dimensional Sagittal Plane Patello-Femoral Model: Comparing Model Approximation to In Vivo Measurement," Comput. Methods Biomech. Biomed. Eng. (in press).
[23] Lund, M. E., de Zee, M., Andersen, M. S., and Rasmussen, J., 2012, "On Validation of Multibody Musculoskeletal Models," Proc. Inst. Mech. Eng. Part H, **226**(2), pp. 82–94.
[24] Roberts, T. J., and Gabaldón, A. M., 2008, "Interpreting Muscle Function From EMG: Lessons Learned From Direct Measurements of Muscle Force," Integr. Comp. Biol., **48**(2), pp. 312–320.
[25] Meyer, A. J., D'Lima, D. D., Besier, T. F., Lloyd, D. G., Colwell, C. W., and Fregly, B. J., 2013, "Are External Knee Load and EMG Measures Accurate Indicators of Internal Knee Contact Forces During Gait?," J. Orthop. Res., **31**(6), pp. 921–929.
[26] Herzog, W., Longino, D., and Clark, A., 2003, "The Role of Muscles in Joint Adaptation and Degeneration," Langenbecks Arch. Surg., **388**(5), pp. 305–315.
[27] Thelen, D. G., Choi, K. W., and Schmitz, A. M., 2014, "Co-Simulation of Neuromuscular Dynamics and Knee Mechanics During Human Walking," ASME J. Biomech. Eng., **136**(2), p. 021033.
[28] Guess, T. M., Stylianou, A. P., and Kia, M., 2014, "Concurrent Prediction of Muscle and Tibiofemoral Contact Forces During Treadmill Gait," ASME J. Biomech. Eng., **136**(2), p. 021032.
[29] Kia, M., Stylianou, A. P., and Guess, T. M., 2014, "Evaluation of a Musculoskeletal Model With Prosthetic Knee Through Six Experimental Gait Trials," Med. Eng. Phys., **36**(3), pp. 335–344.
[30] Hast, M. W., and Piazza, S. J., 2013, "Dual-Joint Modeling for Estimation of Total Knee Replacement Contact Forces During Locomotion," ASME J. Biomech. Eng., **135**(2), p. 021013.
[31] Andersen, M. S., and Rasmussen, J., 2011, "Total Knee Replacement Musculoskeletal Model Using a Novel Simulation Method for Non-Conforming Joints," Proceedings of the International Society of Biomechanics Conference, International Society of Biomechanics, ISB, Brussels.
[32] Pellikaan, P., van der Krogt, M., Carbone, V., Verdonschot, N., and Koopman, B., 2012, "Are Muscle Volumes Linearly Scalable in Musculoskeletal Models?," J. Biomech., **45**(1), p. S498.
[33] Carbone, V., van der Krogt, M., Koopman, B., and Verdonschot, N., 2012, "Functional Scaling of Subject-Specific Musculo-Tendon Parameters in the Lower Extremity," J. Biomech., **45**(1), p. S492.
[34] Redert, A., Kaptein, B., Reinders, M., van den Eelaart, I., and Hendriks, E., 1999, "Extraction of Semantic 3D Models of Human Faces From Stereoscopic Image Sequences," Acta Stereol., **18**, pp. 255–264.
[35] Pellikaan, P., van der Krogt, M. M., Carbone, V., Fluit, R., Vigneron, L. M., Van Deun, J., Verdonschot, N., and Koopman, H. F. J. M., 2014, "Evaluation of a Morphing Based Method to Estimate Muscle Attachment Sites of the Lower Extremity," J. Biomech., **47**(5), pp. 1144–1150.
[36] Kirking, B., Krevolin, J., Townsend, C., Colwell, C. W., and D'Lima, D. D., 2006, "A Multiaxial Force-Sensing Implantable Tibial Prosthesis," J. Biomech., **39**(9), pp. 1744–1751.
[37] Damsgaard, M., Rasmussen, J., Christensen, S. T., Surma, E., and de Zee, M., 2006, "Analysis of Musculoskeletal Systems in the Anybody Modeling System," Simul. Modell. Pract. Theory, **14**(8), pp. 1100–1111.
[38] Carbone, V., Fluit, R., Pellikaan, P., van der Krogt, M. M., Janssen, D., Damsgaard, M., Vigneron, L., Feilkas, T., Koopman, H. F. J. M., and Verdonschot, N., 2014, "TLEM 2.0—A Comprehensive Musculoskeletal Geometry Dataset for Subject-Specific Modeling of Lower Extremity," J. Biomech. (accepted).
[39] Parra, W. C. H., Chatterjee, H. J., and Soligo, C., 2012, "Calculating the Axes of Rotation for the Subtalar and Talocrural Joints Using 3D Bone Reconstructions," J. Biomech., **45**(6), pp. 1103–1107.
[40] Rasmussen, J., Zee, M. de, Damsgaard, M., Christensen, S. T., Marek, C., and Siebertz, K., 2005, "A General Method for Scaling Musculo-Skeletal Models," 2005 International Symposium on Computer Simulation in Biomechanics, Cleveland, OH.
[41] Andersen, M. S., Damsgaard, M., MacWilliams, B., and Rasmussen, J., 2010, "A Computationally Efficient Optimisation-Based Method for Parameter Identification of Kinematically Determinate and Over-Determinate Biomechanical Systems," Comput. Methods Biomech. Biomed. Eng., **13**(2), pp. 171–183.
[42] Zajac, F. E., 1989, "Muscle and Tendon: Properties, Models, Scaling, and Application to Biomechanics and Motor Control," Crit. Rev. Biomed. Eng., **17**(4), pp. 359–411.
[43] Silva, M., Shepherd, E. F., Jackson, W. O., Pratt, J. A., McClung, C. D., and Schmalzried, T. P., 2003, "Knee Strength After Total Knee Arthroplasty," J. Arthroplasty, **18**(5), pp. 605–611.
[44] Rasmussen, J., Damsgaard, M., and Voigt, M., 2001, "Muscle Recruitment by the Min/Max Criterion—A Comparative Numerical Study," J. Biomech., **34**(3), pp. 409–415.
[45] Holmberg, L. J., and Klarbring, A., 2011, "Muscle Decomposition and Recruitment Criteria Influence Muscle Force Estimates," Multibody Syst. Dyn., **28**(3), pp. 283–289.
[46] Happee, R., and Van Der Helm, F. C. T., 1995, "The Control of Shoulder Muscles During Goal Directed Movements, an Inverse Dynamic Analysis," J. Biomech., **28**(10), pp. 1179–1191.
[47] Andersen, M. S., Damsgaard, M., and Rasmussen, J., 2009, "Kinematic Analysis of Over-Determinate Biomechanical Systems," Comput. Methods Biomech. Biomed. Eng., **12**(4), pp. 371–384.
[48] Benoit, D. L., Ramsey, D. K., Lamontagne, M., Xu, L., Wretenberg, P., and Renström, P., 2006, "Effect of Skin Movement Artifact on Knee Kinematics During Gait and Cutting Motions Measured In Vivo," Gait Posture, **24**(2), pp. 152–164.
[49] Andersen, M. S., Benoit, D. L., Damsgaard, M., Ramsey, D. K., and Rasmussen, J., 2010, "Do Kinematic Models Reduce the Effects of Soft Tissue Artefacts in Skin Marker-Based Motion Analysis? an In Vivo Study of Knee Kinematics," J. Biomech., **43**(2), pp. 268–273.
[50] Andersen, M. S., Damsgaard, M., and Rasmussen, J., 2011, "Force-Dependent Kinematics: A New Analysis Method for Non-Conforming Joints," XIII International Symposium on Computer Simulation in Biomechanics, Leuven, Belgium.
[51] Bowman, K. F., and Sekiya, J. K., 2010, "Anatomy and Biomechanics of the Posterior Cruciate Ligament, Medial and Lateral Sides of the Knee," Sports Med. Arthrosc., **18**(4), pp. 222–229.
[52] Chwaluk, A., and Ciszek, B., 2009, "Anatomy of the Posterior Cruciate Ligament," Folia Morphol. (Warsaw), **68**(1), pp. 8–12.
[53] Starok, M., Lenchik, L., Trudell, D., and Resnick, D., 1997, "Normal Patellar Retinaculum: MR and Sonographic Imaging With Cadaveric Correlation," AJR, Am. J. Roentgenol., **168**(6), pp. 1493–1499.

[54] Baldwin, J. L., 2009, "The Anatomy of the Medial Patellofemoral Ligament," Am. J. Sports Med., **37**(12), pp. 2355–2361.
[55] Desio, S. M., Burks, R. T., and Bachus, K. N., 1998, "Soft Tissue Restraints to Lateral Patellar Translation in the Human Knee," Am. J. Sports Med., **26**(1), pp. 59–65.
[56] Dopirak, R. M., Steensen, R. N., and Maurus, P. B., 2008, "The Medial Patellofemoral Ligament," Orthopedics, **31**(4), pp. 331–338.
[57] Philippot, R., Boyer, B., Testa, R., Farizon, F., and Moyen, B., 2012, "The Role of the Medial Ligamentous Structures on Patellar Tracking During Knee Flexion," Knee Surg. Sports Traumatol. Arthrosc., **20**(2), pp. 331–336.
[58] Heegaard, J., Leyvraz, P. F., Van Kampen, A., Rakotomanana, L., Rubin, P. J., and Blankevoort, L., 1994, "Influence of Soft Structures on Patellar Three-Dimensional Tracking," Clin. Orthop. Relat. Res., **299**, pp. 235–243.
[59] Nomura, E., Horiuchi, Y., and Kihara, M., 2000, "Medial Patellofemoral Ligament Restraint in Lateral Patellar Translation and Reconstruction," Knee, **7**(2), pp. 121–127.
[60] Amis, A. A., Firer, P., Mountney, J., Senavongse, W., and Thomas, N. P., 2003, "Anatomy and Biomechanics of the Medial Patellofemoral Ligament," Knee, **10**(3), pp. 215–220.
[61] Blankevoort, L., Kuiper, J. H., Huiskes, R., and Grootenboer, H. J., 1991, "Articular Contact in a Three-Dimensional Model of the Knee," J. Biomech., **24**(11), pp. 1019–1031.
[62] Butler, D. L., Kay, M. D., and Stouffer, D. C., 1986, "Comparison of Material Properties in Fascicle-Bone Units From Human Patellar Tendon and Knee Ligaments," J. Biomech., **19**(6), pp. 425–432.
[63] Conlan, T., Garth, W. P., and Lemons, J. E., 1993, "Evaluation of the Medial Soft-Tissue Restraints of the Extensor Mechanism of the Knee," J. Bone Jt. Surg. Am., **75**, pp. 682–693.
[64] Sprague, M. A., and Geers, T. L., 2003, "Spectral Elements and Field Separation for an Acoustic Fluid Subject to Cavitation," J. Comput. Phys., **184**(1), pp. 149–162.
[65] Schwer, L. E., 2007, "Validation Metrics for Response Histories: Perspectives and Case Studies," Eng. Comput., **23**(4), pp. 295–309.
[66] Chen, Z., Zhang, X., Ardestani, M. M., Wang, L., Liu, Y., Lian, Q., He, J., Li, D., and Jin, Z., 2014, "Prediction of In Vivo Joint Mechanics of an Artificial Knee Implant Using Rigid Multi-Body Dynamics With Elastic Contacts," Proc. Inst. Mech. Eng. Part H, **228**(6), pp. 564–575.
[67] Shelburne, K. B., Torry, M. R., and Pandy, M. G., 2006, "Contributions of Muscles, Ligaments, and the Ground-Reaction Force to Tibiofemoral Joint Loading During Normal Gait," J. Orthop. Res., **24**(10), pp. 1983–1990.
[68] Anderson, F. C., and Pandy, M. G., 2003, "Individual Muscle Contributions to Support in Normal Walking," Gait Posture, **17**(2), pp. 159–169.
[69] Li, G., Zayontz, S., Most, E., Otterberg, E., Sabbag, K., and Rubash, H. E., 2001, "Cruciate-Retaining and Cruciate-Substituting Total Knee Arthroplasty: An In Vitro Comparison of the Kinematics Under Muscle Loads," J. Arthroplasty, **16**(8), pp. 150–156.
[70] Lin, Y.-C., Walter, J. P., Banks, S. A., Pandy, M. G., and Fregly, B. J., 2010, "Simultaneous Prediction of Muscle and Contact Forces in the Knee During Gait," J. Biomech., **43**(5), pp. 945–952.
[71] Kim, H. J., Fernandez, J. W., Akbarshahi, M., Walter, J. P., Fregly, B. J., and Pandy, M. G., 2009, "Evaluation of Predicted Knee-Joint Muscle Forces During Gait Using an Instrumented Knee Implant," J. Orthop. Res., **27**(10), pp. 1326–1331.
[72] Martelli, S., Valente, G., Viceconti, M., and Taddei, F., 2014, "Sensitivity of a Subject-Specific Musculoskeletal Model to the Uncertainties on the Joint Axes Location," Comput. Methods Biomech. Biomed. Eng., pp. 1–9.
[73] Correa, T. A., and Pandy, M. G., 2011, "A Mass-Length Scaling Law for Modeling Muscle Strength in the Lower Limb," J. Biomech., **44**(16), pp. 2782–2789.
[74] Lin, Y.-C., Haftka, R. T., Queipo, N. V., and Fregly, B. J., 2010, "Surrogate Articular Contact Models for Computationally Efficient Multibody Dynamic Simulations," Med. Eng. Phys., **32**(6), pp. 584–594.
[75] Sheehan, F. T., and Drace, J. E., 2000, "Human Patellar Tendon Strain. A Noninvasive, In Vivo Study," Clin. Orthop. Relat. Res., **370**, pp. 201–217.
[76] Athwal, K. K., Hunt, N. C., Davies, A. J., Deehan, D. J., and Amis, A. A., 2014, "Clinical Biomechanics of Instability Related to Total Knee Arthroplasty," Clin. Biomech. (Bristol, Avon), **29**(2), pp. 119–128.
[77] Hughes, R., Bean, J., and Chaffin, D., 1995, "Evaluating the Effect of Co-Contraction in Optimization Models," J. Biomech., **2**(7), pp. 875–878.